A Simple Ring Current Model for Describing In-Plane Aromaticity in Pericyclic Reactions

Iñaki Morao and Fernando P. Cossío*

Kimika Fakultatea, Euskal Herriko Unibertsitatea, P.K. 1072, 20080 San Sebastián-Donostia, Spain

Received September 15, 1998

The ring current model allows the characterization of the in-plane aromaticity present in the transition structures of several pericyclic reactions. The differences between in-plane and π aromaticity can be readily characterized by means of this model. In the presence of a magnetic field, in-plane aromaticity is manifested by a ring current moving along the molecular plane, thus yielding a maximum diamagnetic shielding at the ring point of the electron density. This shielding decays monotonically above and below the molecular plane. In contrast, π aromaticity can be characterized by two ring currents moving at a certain distance above and below the molecular plane. This distance corresponds to the covalent radius of the atoms involved. Therefore, the diamagnetic shielding is not maximum at the ring point of the electron density.

Introduction

The concept of aromaticity has been the object of renewed interest in recent years.[1] In effect, despite the importance of aromaticity in chemistry, its definition is not free of ambiguities, and several definitions have been proposed.[1,2] Among them, those based on magnetic criteria have found wide application since several computational tools have been developed to compute magnetic exaltations,[3] magnetic anisotropies[3,4] or, more recently, nucleus-independent chemical shifts (NICS).[5] This latter method, introduced by Schleyer, provides an absolute scale for the characterization of aromaticity. In general, the magnetic properties of aromatic compounds, namely, large magnetic susceptibility exaltations and anisotropies, as well as large negative NICS values at the center of the rings, are attributed to cyclic π-electron delocalization.[6] Moreover, because aromaticity has also been involved in the development of the theory of pericyclic reactions,[7] these ideas can be readily extended to transition structures associated with thermally allowed pericyclic reactions.[8]

Recently, the ring current model has become a very useful tool for the interpretation of the properties of aromatic compounds,[9] particularly their NMR spectra.[10] Although this model has been criticized,[9] recent careful computational studies[11,12] support, at least partially, its validity. For example, computation of current density maps has revealed appreciable ring currents in aromatic hydrocarbons, heterocycles,[12] and related compounds, whereas it has shown the nonaromatic character of borazine and boroxine. This result has also been confirmed by Schleyer et al. on the basis of NICS data.[13]

If the concept of aromaticity is not free from ambiguities, the idea of in-plane aromaticity is even more difficult to quantify[14] and has been restricted to small rings[15] and unsaturated cyclic hydrocarbons or ions.[16] In this context, we have recently reported[17] in a preliminary note that the evaluation of the NICS at the center of a cyclic saddle point and its variation along the axis perpendicular to the molecular plane reflects the in-plane aromatic character of the transition structures of 1,3-dipolar cycloadditions. In the present paper, we extend these ideas to several pericyclic reactions and we demostrate that the behavior of the NICS along the axis determined by the external magnetic field can be readily

(1) Minkin, V. I.; Glukhotsev, M. N.; Simkin, B. Y. *Aromaticity and Antiaromaticity: Electronic and Structural Aspects*; Wiley: New York, 1994.

(2) Schleyer, P. v. R.; Jiao, H. *Pure Appl. Chem.* **1996**, *68*, 209 and references therein.

(3) See for example: (a) Schleyer, P. v. R.; Freeman, P.; Jiao, H.; Goldfuss, B. *Angew. Chem., Int. Ed. Engl.* **1995**, *34*, 337. (b) Dauben, H. J., Jr.; Wilson, J. D.; Laity, J. L. *J. Am. Chem. Soc.* **1968**, *90*, 811.

(4) See for example: (a) Benson, R. C.; Flygare, W. H. *J. Am. Chem. Soc.* **1970**, *92*, 7523. (b) Schmalz, T. G.; Norris, C. L.; Flygare, W. H. *J. Am. Chem. Soc.* **1973**, *95*, 7961.

(5) Schleyer, P. v. R.; Maerker, C.; Dransfed, A.; Jiao, H.; Hommes N. J. R. v. E. *J. Am. Chem. Soc.* **1996**, *118*, 6317.

(6) However, this π delocalization can be a consequence of bond equalization of the σ framework. See for example: (a) Hiberty, P. C.; Danovich, D.; Shurki, A.; Shaik, S. *J. Am. Chem. Soc.* **1995**, *117*, 7760 and references to previous work therein. (b) Gobbi, A.; Yamaguchi, Y.; Frenking, G.; Schaefer, H. F., III. *Chem Phys. Lett.* **1995**, *244*, 27. For a view based on the π framework, see: (c) Baird, N. C. *J. Org. Chem.* **1986**, *51*, 3907. (d) Wiberg, K. B.; Nakaji, D.; Breneman, C. *J. Am. Chem. Soc.* **1989**, *11*, 4178.

(7) (a) Evans, M. G.; Warhurst, E. *Trans. Faraday Soc.* **1938**, *34*, 614. (b) Zimmerman, H. E. *Acc. Chem. Res.* **1971**, *4*, 272.

(8) See for example: (a) Herges, R.; Jiao, H.; Schleyer, P. v. R. *Angew. Chem., Int. Ed. Engl.* **1994**, *33*, 1376. (b) Jiao, H.; Schleyer, P. v. R. *Angew. Chem., Int. Ed. Engl.* **1993**, *32*, 1763. (c) Jiao, H.; Schleyer, P. v. R. *Angew. Chem., Int. Ed. Engl.* **1995**, *34*, 334. (d) Jiao, H.; Schleyer, P. v. R. *J. Chem. Soc., Perkins Trans. 2* **1994**, 407. (e) Jiao, H.; Schleyer, P. v. R. *J. Am. Chem. Soc.* **1995**, *117*, 11529.

(9) Haig, C. W.; Maillon, R. B. *Prog. Nucl. Magn. Reson. Spectrosc.* **1980**, *13*, 303 and references therein.

(10) Pauling, L. *J. Chem. Phys.* **1936**, *4*, 673. (b) London, F. *J. Phys. Radium* **1937**, *8*, 397. (c) Pople, J. A. *J. Chem. Phys.* **1956**, *24*, 1111. (d) Schneider, W. G.; Bernstein, H. J.; Pople, J. A. *J. Am. Chem. Soc.* **1958**, *80*, 3497.

(11) Fleischer, U.; Kutzelnigg, W.; Lazzaretti, P.; Muhllenkamp, V. *J. Am. Chem. Soc.* **1974**, *116*, 5298.

(12) Fowler, P. W.; Steiner, E. *J. Phys. Chem.* **1997**, *101*, 1409.

(13) Schleyer, P. v. R.; Jiao, H.; Hommes, N. J. R. v. E.; Malkin, V. G.; Malkina, O. L. *J. Am. Chem. Soc.* **1997**, *119*, 12669.

(14) (a) Chandrasekhar, J.; Jemmis, E. D.; Schleyer, P. v. R. *Tetrahedron Lett.* **1979**, 3707. (b) Dewar, M. J. S. *J. Am. Chem. Soc.* **1984**, *106*, 669.

(15) (a) Cremer, D. *Tetrahedron* **1988**, *44*, 7427. (b) Cremer, D.; Kraka, E. *J. Am. Chem. Soc.* **1986**, *108*, 7467. (c) Burk, P.; Abboud, J.-L. M.; Koppel, I. A. *J. Phys. Chem.* **1996**, *100*, 6992.

(16) (a) Schleyer, P. v. R.; Jiao, H.; Glukhovtsev, M. N.; Chandrasekhar, J.; Kraka, E. *J. Am. Chem. Soc.* **1994**, *116*, 10129. (b) McEwen, A. B.; Schleyer, P. v. R. *J. Org. Chem.* **1986**, *51*, 4357.

(17) Morao, I.; Lecea, B.; Cossío, F. P. *J. Org. Chem.* **1997**, *62*, 7033.

10.1021/jo981862+ CCC: $18.00
Published on Web 03/19/1999

rationalized on the basis of the diamagnetic shielding induced by a ring current.

Computational Methods

All of the geometry optimizations and energy calculations have been performed using the GAUSSIAN94 suite of programs.[18] To perform all the calculations at a homogeneous computational level that provides quantitative accuracy at a reasonable computational cost, all of the calculations described in this paper have been performed using Becke's hybrid three parameter functional (B3LYP)[19] and the 6-31+G* basis set.[20] This level of theory has been proven to yield accurate activation parameters and geometries.[17,21] All stationary points were characterized by harmonic analysis. The zero-point vibrational energies (ZPVE) were computed at the B3LYP/6-31+G* or UB3LYP/6-31+G* levels and were not scaled. All of the relative energies reported in this paper include the ZPVE corrections.

Magnetic susceptibility anisotropies (χ_{anis}) have been calculated according to the following equation:

$$\chi_{anis} = \chi_{zz} - \frac{1}{2}[\chi_{xx} + \chi_{yy}] \quad (1)$$

where χ_{zz} is the out-of-plane component and χ_{xx} and χ_{yy} are the in-plane components of the magnetic susceptibility tensor. These values were computed using the continuous set of gauge transformations (CSGT)[22] method. The NICS were computed by means of the gauge-independent atomic orbital (GIAO)[23] method.

Results and Discussion

General Model. Let us consider an external magnetic field $\mathbf{B_o}$ oriented along the *z* axis and a ring current *A* circulating along the *xy* plane, which corresponds to the molecular plane (see Figure 1). According to quantum theory,[24] the magnitude of the diamagnetic shielding constant along the *z* axis σ^d_{zz} is given by

$$\sigma^d_{zz} = -\frac{e^2\mu_0}{8\pi m_e}\int\left(\frac{x^2+y^2}{r^3}\right)\Psi_0{}^2 d\tau \quad (2)$$

where all the symbols have their usual meaning. Assuming a circular trajectory for the ring current *A*, it follows that

$$\Psi_0{}^2 = (2\pi R_{av})^{-1} \quad (3)$$

where R_{av} is the average distance of the ring current to the center of the ring (vide infra). Under this simplified scheme, the value of σ^d_{zz} along the *z*-axis can be readily evaluated and eq 2 becomes

$$\sigma^d_{zz} = -\frac{e^2\mu_0}{8\pi m_e}R_{av}{}^{-1}\left[1+\left(\frac{z}{R_{av}}\right)^2\right]^{-3/2} \quad (4)$$

According to eq 4, the maximum diamagnetic shielding occurs in the molecular plane ($z = 0$) and therefore

$$\sigma^d_{max} = -\frac{e^2\mu_0}{8\pi m_e}R_{av}{}^{-1} \quad (5)$$

Similarly, for an out-of-plane ring current *B* circulating at a R_0 distance above or below the molecular plane (Figure 1), we obtain

$$\sigma^d_{zz} = -\frac{e^2\mu_0}{8\pi m_e}R_{av}{}^{-1}\left[1+\left(\frac{z-R_0}{R_{av}}\right)^2\right]^{-3/2} \quad (6)$$

In this case, σ^d_{max} is reached when $z = R_o$.

From eq 5, it is clear that the magnitude of the diamagnetic shielding decreases with the size of the ring, although this decrease is slower than that associated with other parameters that depend on the inverse of the area of the ring, such as magnetic exaltation.[3] Therefore, the diamagnetic shielding is less sensitive to the size of the cyclic system under consideration, as it has been reported by Schleyer et al.[5,13]

Although the total magnitude of the shielding constant depends not only on diamagnetic currents but also on local effects and paratropic currents,[11−13] the variation of these effects should be less important than that of the diamagnetic ring current, and their magnitude should be even lower along the *z*-axis. Therefore, if the ring current model is valid, the $\sigma^d_{zz}/\sigma^d_{max}$ vs *z* and the NICS/$NICS_{max}$ vs *z* curves must be similar:

$$\frac{\sigma^d_{zz}}{\sigma^d_{max}} \approx \frac{NICS}{NICS_{max}} \quad (7)$$

In addition, the shapes of both the $\sigma^d_{zz}/\sigma^d_{max}$ vs *z* and the NICS/$NICS_{max}$ vs *z* curves should be different for in-plane and π ring currents associated with aromatic structures. In the next subsections, we will apply these ideas to several pericyclic reactions, and we will show how this

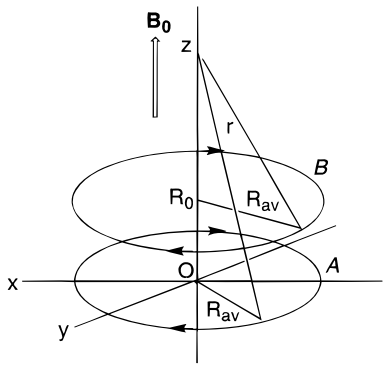

Figure 1. Graphical definition of the geometric parameters included in eqs 2−6. The $z = 0$ plane is the molecular plane. Trajectories *A* and *B* define in-plane and out-of-plane ring currents, respectively.

(18) *Gaussian 94*, Revision B.2; Frisch, M. J.; Trucks, G. W.; Schlegel, H. B.; Gill, P. M. W.; Johnson, B. G.; Robb, M. A.; Cheeseman, J. R.; Keith, T.; Petersson, G. A.; Montgomery, J. A.; Raghavachari, K.; Al-Laham, M. A.; Zakrzewski, V. G.; Ortiz, J. V.; Foresman, J. B.; Peng, C. Y.; Ayala, P. Y.; Chen, W.; Wong, M. W.; Andres, J. L.; Replogle, E. S.; Gomperts, R.; Martin, R. L.; Fox, D. J.; Binkley, J. S.; Defrees, D. J.; Baker, J.; Stewart, J. S.; Head-Gordon, M.; Gonzalez, C.; Pople, J. A.; Gaussian, Inc.: Pittsburgh, PA, 1995.

(19) (a) Becke, A. D. *J. Chem. Phys.* **1993**, *98*, 5648. (b) Lee, C.; Yang, W.; Parr, P. G. *Phys. Rev. A* **1988**, *38*, 3098.

(20) Frisch, M. J.; Pople, J. A.; Binkley, J. S. *J. Chem. Phys.* **1994**, *80*, 3265.

(21) (a) Wiest, O.; Black, K. A.; Houk, K. N. *J. Am. Chem. Soc.* **1994**, *116*, 10336. (b) Wiest, O.; Houk, K. N.; Black, K. A.; Thomas, B., IV. *J. Am Chem. Soc.* **1995**, *117*, 8594. (c) Goldstein, E.; Beno, B.; Houk, H. N. *J. Am. Chem. Soc.* **1996**, *118*, 6036.

(22) (a) Keith, T. A.; Bader, R. F. W. *Chem Phys. Lett.* **1993**, *210*, 223. (b) Keith, T. A.; Bader, R. F. W. *Chem. Phys. Lett.* **1992**, *194*, 1.

(23) Wolinski, K.; Hilton, J. F.; Pulay, P. *J. Am. Chem. Soc.* **1990**, *112*, 8251.

(24) Atkins, P. W.; Friedman, R. S. *Molecular Quantum Mechanics*; Oxford University Press: Oxford, 1997; pp 431−432.

Scheme 1

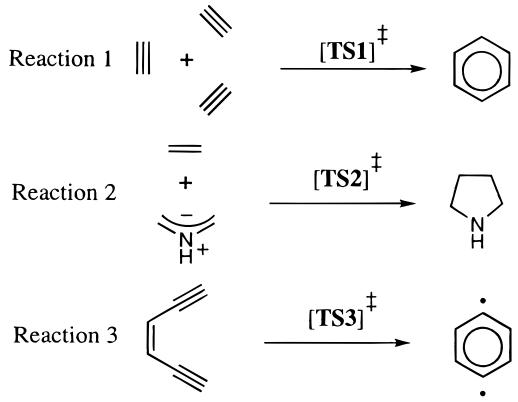

simple current model accounts for in-plane aromaticity in the corresponding transitions structures.

Trimerization of Acetylene. We first studied the trimerization of acetylene to form benzene (Scheme 1, reaction 1). This reaction has attracted the attention of both theoretical and experimental chemists since Berthelot reported in 1866 that reaction of acetylene at 600 °C yielded small amounts of benzene.[25] However, it has been demostrated that the reaction requires the assistance of transition-metal catalysts to proceed in useful yields.[26] Indeed, Vollhardt et al. [27] have shown that even when benzene-like compounds are obtained via thermal isomerization of triynes, formation of these products takes place via consecutive sigmatropic shifts rather than through [2 + 2 + 2] cycloadditions. Actually, only the corresponding cycloreversion reaction has been observed by Vollhardt in the special case of an strained 1,3,6-cyclohexatriene.[28] These observations have intrigued both theoreticians and experimentalists, because according to the Woodward−Hoffmann rules, the supra−supra pathway is thermally allowed[29] and the high exothermicity of the reaction[30] (ΔH°_{rxn} = −142.76 kcal/mol) should favor benzene formation under thermodynamic control. Several theoretical papers[31−33] have been reported to account for the inherent kinetic difficulty of this reaction. The high activation energies observed at the different computational levels have been attributed to repulsive four-electron interations between the out-of-plane π bonds at the transition structure[31] or to the additional energetic requirements needed to combine three reactive fragments.[32] More recently, Birney et al.[33] have found that any hypothetical π-stabilization at the transition state should be weak.

We have located and caracterized the **TS1** saddle point at the B3LYP/6-31+G* level. Its geometrical features are

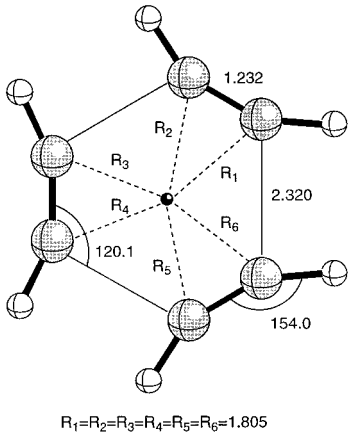

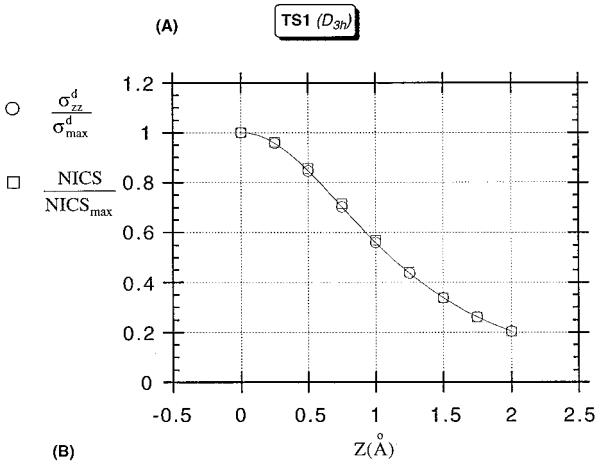

Figure 2. (A) Fully optimized B3LYP/6-31+G* geometry of **TS1** associated with trimerization of acetylene. Bond angles and distances are given in Å and deg, respectively. The central point is the (3,+1) ring point of electron density. (B) Plots of the $\sigma^d_{zz}/\sigma^d_{max}$ vs *z* and the NICS/NICSmax vs *z* curves for **TS1**. The *z*-axis is perpendicular to the molecular plane and intercepts the (3,+1) ring point. The NICS/NICSmax data have been computed at the GIAO-SCF/6-31+G*//B3LYP/6-31+G* level.

reported in Figure 2A. At this computational level, **TS1** has D_{3h} symmetry, in agreement with previously reported structures.[31−33] Our computed activation energy (Table 1) is between those obtained by Birney[33] at the MP2/6-31+G* and MP4SDT(Q)/6-31+G*//MP2/6-31+G*+ZPVE levels, 45.0 and 51.4 kcal/mol, respectively. Similarly, our calculated reaction energy and enthalpy are ca. 6% larger than the experimental estimate.[30]

We have investigated the aromatic character of **TS1** by computing the NICS at the (3,+1) ring point of electron density,[34] because this is the most appropriate point to characterize a ring unambiguously.[17,34] In this case, given the D_{3h} symmetry of **TS1**, the ring point is the center of masses. Our computed NICS at the GIAO-SCF/6-31+G*//B3LYP/6-31+G* level is −15.06 ppm, a quite large value which parallels the large values of magnetic susceptibility anisotropies (see the χ_{anis} and $\Delta\chi_{anis}$ values in Table 1). Therefore, we can conclude that **TS1** is aromatic. To test its in-plane aromatic character, we have computed the NICS along the *z*-axis which intersects the (3,+1) point and is perpendicular to the

(25) Berthelot, M. C. R. *Séanc. Acad. Sci.* **1866**, *62*, 905.
(26) Schore, N. E. In *Comprehensive Organic Synthesis*; Trost, B. M., Fleming, I., Eds.; Pergamon: Oxford, 1991; Vol. 5, pp 1144−1152.
(27) Dower, W. V.; Vollhardt, K. P. C. *Tetrahedron* **1986**, *42*, 1873.
(28) Diercks, R.; Vollhardt, K. P. C. *J. Am. Chem. Soc.* **1986**, *108*, 3150.
(29) Woodward, R. B.; Hoffmann, R. *The Conservation of Orbital Symmetry*; Academic Press: New York, 1970.
(30) (a) Chase, M. W.; Davies, J. R.; Downey, D. R.; Frurip, R. A.; McDonald, R. A.; Syvervd, A. N. *JANAF Thermochemical Tables, Third Ed., J. Phys. Chem. Ref. Data* **1985**, *14*, Suppl. 1. (b) Cox, J. O.; Pilcher, G. *Thermochemistry of Organic and Organometallic Compounds*; Academic Press: New York, 1970.
(31) (a) Bach, R. D.; Wolber, J. W.; Schlegel, H. B. *J. Am. Chem. Soc.* **1985**, *107*, 2837. (b) Houk, H. N.; Gandour, R. W.; Rondan, N. G.; Paquette, L. A. *J. Am. Chem. Soc.* **1979**, *101*, 6797.
(32) Ioffe, A.; Shaik, S. *J. Chem. Soc., Perkin Trans 2* **1992**, 2101.
(33) Wagenseller, P. E.; Birney, D. M.; Roy, D. *J. Org. Chem.* **1995**, *60*, 2853.
(34) Bader, R. F. W. *Atoms in Molecules-A Quantum Theory*; Clarendon Press: Oxford, 1990; pp 12−52.

Table 1. Calculations for Reactions 1−3 and Transition Structures TS1−3 (Scheme 1)[a]

	reaction or transition structure		
	1	**2**	**3**
ΔE_a (kcal/mol)[b]	48.09	8.45	30.48
ΔE_{rxn} (kcal/mol)[b]	−150.17	−55.98	6.56
$\Delta H^{\ddagger}$ (kcal/mol)[b,c]	48.26	5.29	29.73
ΔH°_{rxn} (kcal/mol)[b,c]	−152.75	−57.36	5.44
R_{av} (Å)[d]	1.452	1.206	1.454
σ^{d}_{max} (ppm)[e]	−9.70	−11.68	−9.69
$NICS_{max}$ (ppm)[f]	−15.06	−20.84	−19.29
χ_{anis} (10^{-6} erg/G^2 mol)[g]	−27.47	−22.03	−36.34
$\Delta\chi_{anis}$[h]	−11.18	−4.06	−33.47

[a] ΔE_a, activation energies; ΔE_{rxn}, reaction energies; $\Delta H^{\ddagger}$, activation enthalpies; ΔH°_{rxn}, enthalpies of reaction; R_{av}, average radii; $\sigma_{max}{}^{d}$, maximum non-local diamagnetic shieldings; $NICS_{max}$, nucleus independent chemical shifts at the corresponding ring points; χ_{anis}, magnetic susceptibility anisotropies. [b] Computed at the B3LYP/6-31+G*+ZPVE level except the reaction 3 values, which were computed at the UB3LYP/6-31+G*+ZPVE level. [c] Computed at 298 K. [d] Computed at the B3LYP/6-31+G* level according to eq 8, except the value corresponding to **TS3**, which was computed at the UB3LYP/6-31+G* level using eq 9 (see text). [e] Computed by means of eq 5. [f] Computed at the GIAO−SCF/6-31+G*//B3LYP/6-31+G* level. [g] Computed at the CSGT-SCF/6-31+G*//B3LYP/6-31+G* level. [h] $\Delta\chi_{anis}$ is the difference between the values of the corresponding transition structures and those of the reactants.

molecular plane. The $NICS/NICS_{max}$ values thus obtained are reported in Figure 2B. We have also computed the $\sigma^{d}_{zz}/\sigma^{d}_{max}$ values along the *z*-axis using eqs 4 and 5 and using the following expresion for the evaluation of R_{av}:

$$R_{av} = n^{-1}\sum_{i=1}^{n}\left(R_i - \frac{4}{Z_i}a_0\right) \qquad (8)$$

where *n* is the number of atoms which participate in the cycloaddition, R_i is the distance from the (3,+1) point to the nucleus *i*, Z_i is the atomic number of the *i*-atom, and a_0 is the Bohr radius. The latter term in eq 8 corresponds to the maximum of the probability of the radial function $4\pi r^2 R_{n,l}{}^2(r)$ for a 2p atomic orbital.

The calculated values of $\sigma^{d}_{zz}/\sigma^{d}_{max}$ along the *z*-axis are also reported in Figure 2B, and the value of σ^{d}_{max} is reported in Table 1. As can be seen, the agreement between the $\sigma^{d}_{zz}/\sigma^{d}_{max}$ data and the $NICS/NICS_{max}$ results is excellent, although σ^{d}_{max} is smaller than the isotropic NICS. This indicates that the high value of $NICS_{max}$ for this reaction is compatible with a ring current circulating along the molecular plane, which is associated with in-plane aromaticity. However, apart from nonlocal effects, other factors contribute to the total isotropic NICS (vide supra). If we consider the reaction product, namely benzene, the σ^{d}_{zz} values can be computed using the usual mean value for R_{av}:

$$R_{av} = n^{-1}\sum_{i=1}^{n}R_i \qquad (9)$$

Using eq 6 and making $R_{av} = 1.398$ Å and $R_0 = 0.75$ Å (which is the covalent radius of carbon),[35] we have obtained the $\sigma^{d}_{zz}/\sigma^{d}_{max}$ vs *z* curve reported in Figure 3B. As can be appreciated, the computed curve is in good agreement with the $NICS/NICS_{max}$ results except when

(35) Pauling, L. *The Nature of the Chemical Bond*, 3rd ed.; Cornell University Press: Ithaca, 1960; p 224.

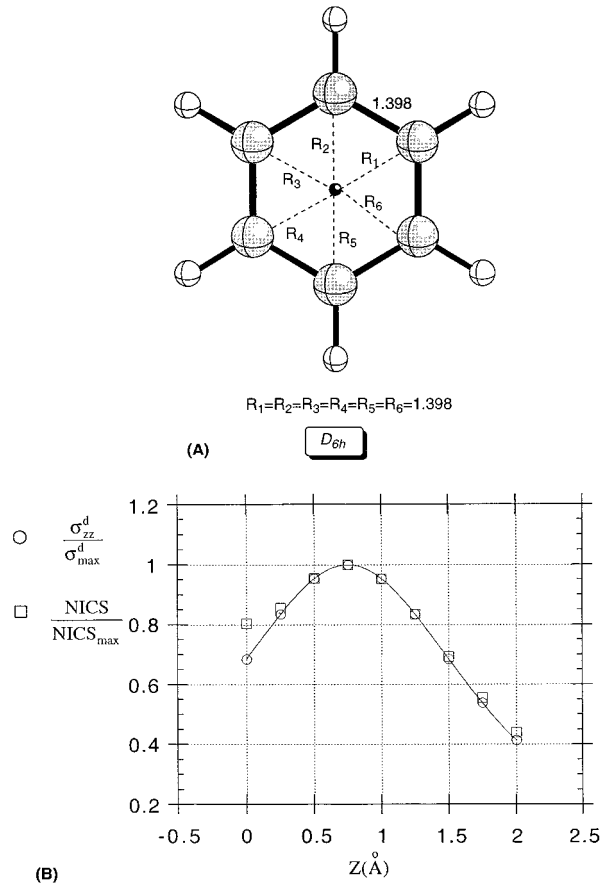

Figure 3. (A) Fully optimized B3LYP/6-31+G* geometry for benzene. See Figure 2 caption for additional details. (B) Plots of the $\sigma^{d}_{zz}/\sigma^{d}_{max}$ vs *z* and the $NICS/NICS_{max}$ vs *z* curves for benzene. See Figure 2 caption for additional details.

$z = 0$. This local disagreement can be explained by taking into account that in the molecular plane ring currents both above and below this plane exert their corresponding diamagnetic effect (vide infra). Apart from this latter point, the shape of both curves is very similar and they exhibit an enhancement until the *z* value associated with the covalent radius of carbon is reached, followed by a decay for larger values. By comparing Figures 2B and 3B, we can readily appreciate the difference between both types of aromaticity. Indeed, we can also conclude that there is no π aromaticity in the transition state corresponding to the trimerization of acetylene. Therefore, in this reaction, the in-plane aromaticity of the transition structure and the π aromaticity of the product are orthogonal to each other, thus resulting in a non-Hammond reaction profile, with large activation and reaction energies.

One reviewer has suggested that the discrepancy between the $NICS/NICS_{max}$ and $\sigma^{d}_{zz}/\sigma^{d}_{max}$ values at $z = 0$ for benzene (vide supra) can be more relevant in other aromatic compounds. In view of this and following the reviewer's suggestion, we have also studied oxazole, a five-membered π-aromatic heterocycle containing two heteroatoms. The fully optimized geometry of oxazole at the B3LYP/6-31+G* level is reported in Figure 4A. In this case, the NICS value at the ring point is found to be −11.32 ppm at the GIAO-SCF/6-31+G*//B3LYP/6-31+G* level. As can be seen in Figure 4B, the NICS value at the ring point is lower than that found at 0.5 Å above or below the molecular plane, although this difference is

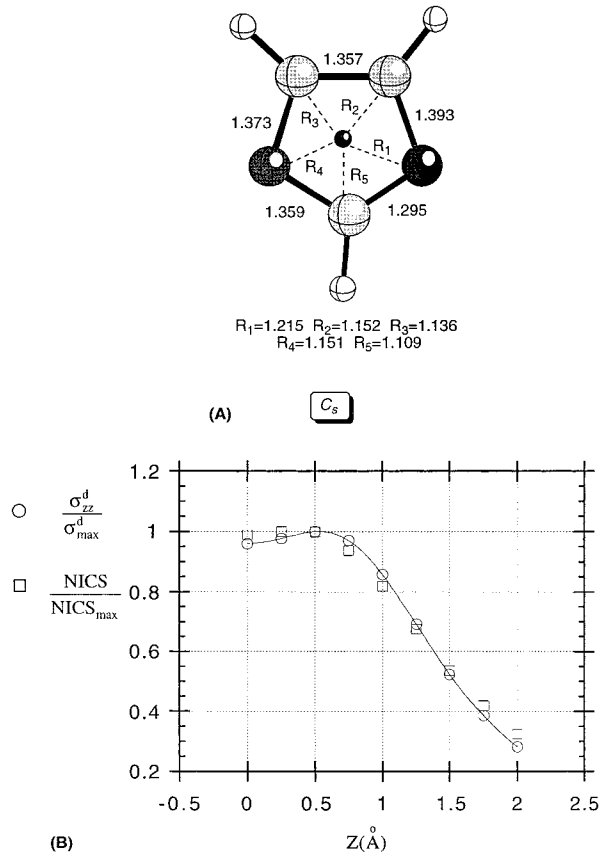

Figure 4. (A) Fully optimized B3LYP/6-31+G* geometry for oxazole. See Figure 2 caption for additional details. (B) Plots of the $\sigma^d_{zz}/\sigma^d_{max}$ vs z and the NICS/NICS$_{max}$ vs z curves for oxazole. See Figure 2 caption for additional details.

significantly lower that that found for benzene. Therefore, this kind of aromatic compound is more sensitive to the diamagnetic effect of two ring currents. If we extend eq 6 to *two* ring currents circulating at a R_0 distance above and below the molecular plane, we arrive at the following expression:

$$\sigma^d_{zz} = -\frac{e^2\mu_0}{16\pi m_e} R_{av}^{-1}\left\{\left[1+\left(\frac{z-R_0}{R_{av}}\right)^2\right]^{-3/2} + \left[1+\left(\frac{z+R_0}{R_{av}}\right)^2\right]^{-3/2}\right\} \quad (10)$$

From the geometric data reported in Figure 4A and using eq 9, we obtain $R_{av} = 1.153$ Å for oxazole. Similarly, the R_0 value can be obtained from the Pauling's radii[35] r_i^{cov} of the involved atoms:

$$R_0 = n^{-1}\sum_{i=1}^{n} r_i^{cov} \quad (11)$$

According to eq 11, for oxazole $R_0 = 0.70$ Å. As can be readily appreciated from Figure 4B, there is an excellent agreement between the NICS/NICS$_{max}$vs z and $\sigma^d_{zz}/\sigma^d_{max}$ vs z curves. The computed NICS$_{max}$ and σ^d_{max} values are −11.45 and −12.21 ppm, respectively. Therefore, the π-aromatic character of oxazole can be described using two ring currents. The reasons for the lower sensitivity of benzene to the second ring current are not clear at present.

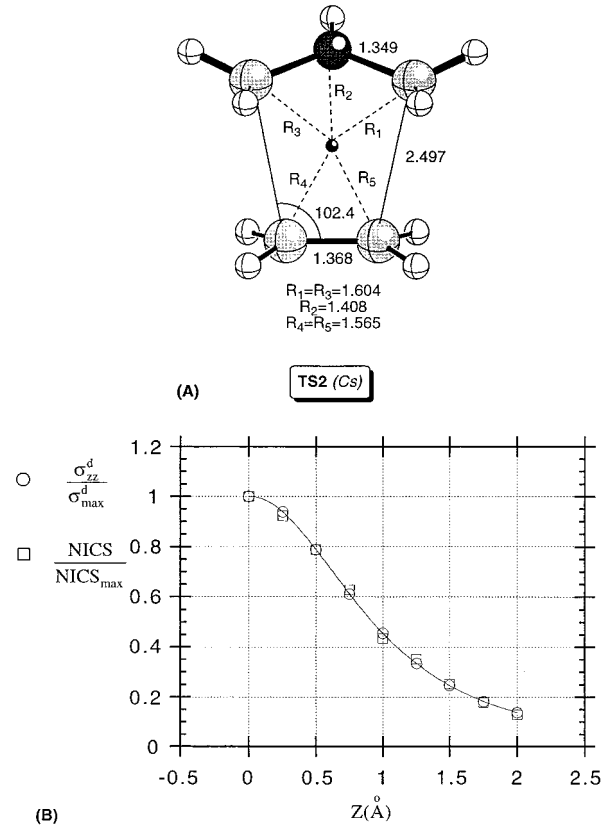

Figure 5. (A) Fully optimized B3LYP/6-31+G* geometry of **TS2** associated with the [3 + 2] cycloaddition reaction between azomethine ylide and ethylene. See Figure 2 caption for additional details. (B) Plots of the $\sigma^d_{zz}/\sigma^d_{max}$ vs z and the NICS/NICS$_{max}$ vs z curves for **TS2**. The z-axis intercepts the (3,+1) point and is perpendicular to the plane defined by the ring point and the ethylene carbon atoms. See Figure 2 caption for additional details.

1,3-Dipolar Cycloaddition between Ethylene and Azomethine Ylide. As an example of [3 + 2] cycloaddition, we have selected the interaction between ethylene and azomethine ylide to form pyrrolidine (Scheme 1, reaction 2). In sharp contrast with the preceding case, this reaction is readily feasible and has found wide application in the chemical synthesis of biologically relevant compounds.[36] We have explored the B3LYP/6-31+G* potential energy surface, and aside from reactants and products, we have located an orientation complex that lies 1.45 kcal/mol below the reactants (see Figure 1 of the Supporting Information), as well as transition structure **TS2**. The activation energy with respect to the complex is calculated to be only 8.45 kcal/mol (Table 1). According to our results, **TS2** has *Cs* symmetry (see Figure 5A). In addition, the high NICS$_{max}$ and χ_{anis} values confirm that this saddle point is aromatic in character (Table 1). The relatively low value of $\Delta\chi_{anis}$ is motivated by the exceptionally large value of the χ_{anis} of azomethine ylide. We calculated the $\sigma^d_{zz}/\sigma^d_{max}$ ratios at various distances, as we did in the previous case, using the R_{av} value

(36) (a) Cinquinni, M.; Cozzi, F. In *Stereoselective Synthesis*; Helmcher, G., Hoffmann, R. W., Mulzer, J., Schaumann, E., Eds.; Thieme: Stuttgart, 1996; Vol. 5, pp 2953−2987. (b) Huisgen, R. In *1,3-Dipolar Cycloaddition Chemistry*; Padwa, A., Ed.; Wiley: New York, 1984; Vol. 1, p 1. (c) Terao, Y.; Aono, M.; Achiwa, K. *Heterocycles* **1988**, *27*, 981. (d) Vedejs, E.; West, F. G. *Chem. Rev.* **1986**, *86*, 941. (e) Padwa, A. In *Comprehensive Organic Synthesis*; Trost, B. M., Fleming, I., Eds.; Pergamon: Oxford, 1991; Vol. 4, pp 1069−1109.

reported in Table 1, which was calculated using eq 4. The resulting data have been collected in Figure 5B. As in the preceding case, an excellent agreement between the NICS/NICS$_{max}$ and the $\sigma^d_{zz}/\sigma^d_{max}$ data is found, despite the departure from planarity of **TS2**. This result indicates that this transition structure also exhibits in-plane aromaticity.

Bergman Rearrangement of (*Z*)-Hex-3-ene-1,5-diyne. Since its discovery by Bergman[37] in 1972, this reaction has been the object of considerable interest because of the presence of the enediyne moiety in diverse families of anticancer reagents.[38] As a consequence, there has been a great deal of research in both the theoretical[39] and experimental[39d,40] fields.

Given the biradical character of the product of this reaction, namely *p*-benzyne (Scheme 1, reaction 3), this reaction has been studied at several multiconfigurational levels, which precludes further computational research on more substituted systems, that would be closer to the compounds of medicinal interest. However, a recent paper from Kraka and Cremer[39c] has shown that the transition structure of this reaction has a negligible biradical character. Therefore, we reasoned that a less computationally demanding theoretical level such as UB3LYP could describe the reaction profile with reasonable accuracy. We have located and characterized a C_{2v} symmetric **TS3** saddle point in the UB3LYP/6-31+G* potential energy surface, which connects (*Z*)-hex-3-ene-1,5-diyne with *p*-benzyne. The chief geometric features of **TS3** have been collected in Figure 6A, and those of the reactant and the product are reported in Figure 2 of the Supporting Information. We have found that at the UB3LYP/6-31+G* level **TS3** has no biradical character and there is no spin contamination. Our computed activation energy and enthalpy (Table 1) are in good agreement with the most recent experimental values determined by Roth et al.[41] ($\Delta E_a = 29.16 \pm 0.5$ kcal/mol, $\Delta H_{rxn} = 28.23 \pm 0.5$ kcal/mol) and are comparable or even better than those computed at considerably more demanding levels.[39] Our computed reaction enthalpy is ca. 3 kcal/mol lower than that determined Roth et al.[41] ($\Delta H_{rxn} = +8.5 \pm 1.0$ kcal/mol). Our computed value[42] for the heat of formation of *p*-benzyne is $\Delta H_f = 135.14$ kcal/mol, and the experimental value is 138.0 ± 1.0 kcal/mol. Therefore, most of the error in our evaluation of the reaction enthalpy comes from the calculated enthalpy of *p*-benzyne. In addition, the UB3LYP/6-31+G* structure of *p*-benzyne shows significant spin contamination ($\langle S^2 \rangle = 0.138$ au), and thereby the quality of the reaction energies is somewhat lower than that of the activation parameters.[43] In any case, this theoretical level describes correctly the reaction profile at a reasonable computational cost and can be used in the study of Bergman rearrangements of larger related molecules.[40,44]

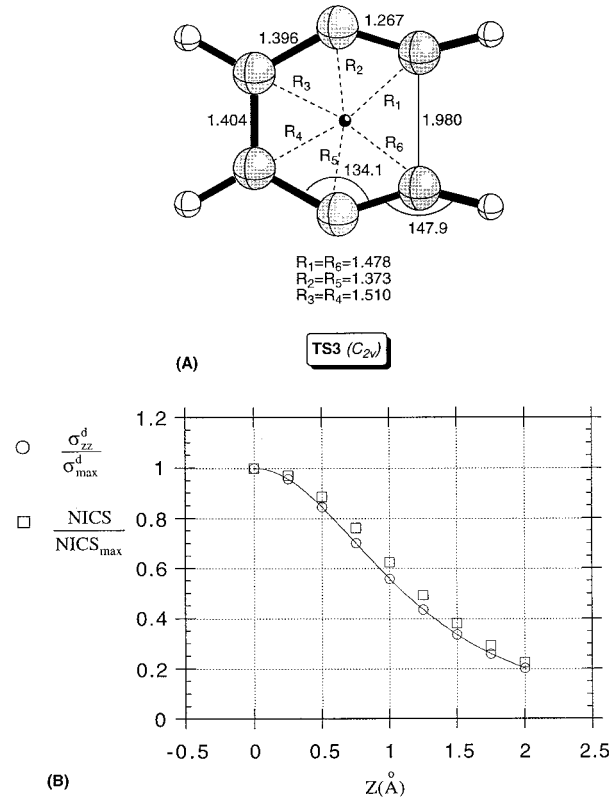

Figure 6. (A) Fully optimized B3LYP/6-31+G* geometry for **TS3** associated with the Bergman reaction of (*Z*)-hex-3-ene-1,5-diyne. See Figure 2 caption for additional details. (B) Plots of the $\sigma^d_{zz}/\sigma^d_{max}$ vs *z* and the NICS/NICS$_{max}$ vs *z* curves for **TS3**. See Figure 2 caption for additional details.

Once we were confident about the quality of our results for **TS3**, we computed its NICS$_{max}$ and χ_{anis} values and found that they correspond to an aromatic stationary point (see Table 1). Given that there is a σ framework in

(37) (a) Jones, R. R.; Bergman, R. G. *J. Am. Chem. Soc.* **1972**, *94*, 660. (b) Lockhart, T. P.; Bergman, R. G. *J. Am. Chem Soc.* **1981**, *103*, 409. (c) Lockhart, T. P.; Commita, P. B.; Bergman, R. G. *J. Am. Chem. Soc.* **1981**, *103*, 4082.

(38) *Enediyne Antibiotics and Antitumor Agents*; Borders, D. B., Doyle, T. E., Eds.; Marcel Dekker: New York, 1995.

(39) (a) Lindh, R.; Lee, T. J.; Bernhardsson, A.; Persson, B. J.; Karlström, G. *J. Am. Chem. Soc.* **1995**, *117*, 7186. (b) Koga, N.; Morokuma, K. *J. Am. Chem. Soc.* **1991**, *113*, 1907. (c) Kraka, E.; Cremer, D. *J. Am. Chem. Soc.* **1994**, *116*, 4929. (d) Hoffner, J.; Schottelius, M. J.; Feichtinger, D.; Chen, P. *J. Am. Chem. Soc.* **1998**, *120*, 376. (e) Lindh, R.; Persson, J. *J. Am. Chem. Soc.* **1994**, *116*, 4946. (f) Snyder, J. P. *J. Am. Chem. Soc.* **1990**, *112*, 5367.

(40) See for example: (a) Nicolaou, K. C.; Ogawa, Y.; Zucarello, G.; Kataoka, H. *J. Am. Chem. Soc.* **1988**, *110*, 7247. (b) Nicolaou, K. C.; Zucarello, G.; Ogawa, Y.; Schweiger, E. J.; Kumazawa, T. *J. Am. Chem. Soc.* **1988**, *110*, 4866. (c) Schreiber, S. L.; Kiessling, L. L. *J. Am. Chem. Soc.* **1988**, *110*, 631. (d) Porco, J. A.; Schoenen, F. J.; Stout, T. J.; Clardy, J.; Schreiber, S. L. *J. Am. Chem. Soc.* **1990**, *112*, 7410. (e) Wood, J. L.; Porco, J. A.; Taunton, J.; Lee, A. Y.; Clardy, J.; Schreiber, S. L. *J. Am. Chem. Soc.* **1992**, *114*, 5898. (f) Elbaum, D.; Porco, J. A.; Stout, T. J.; Clardy, J.; Schreiber, S. L. *J. Am. Chem. Soc.* **1995**, *117*, 211. (g) Magnus, P.; Fortt, S.; Pitterna, T.; Snyder, J. P. *J. Am. Chem. Soc.* **1990**, *112*, 4986.

(41) Roth, W. R.; Hopf, H.; Horn, C. *Chem. Ber.* **1994**, *127*, 1765.

(42) The heat of formation has been calculated according to the following equation:

$$(E)\text{-2-butene} + p\text{-benzyne} \xrightarrow{H^{298}_{rxn}} \text{benzene} + \text{1,3-butadiene}$$

Using the experimental heats of formation of (*E*)-2-butene, benzene, and 1,3-butadiene (-2.7 ± 0.2, 19.8 ± 0.2, and 26.3 kcal/mol, respectively[43]), we have obtained the following expression for the heat of formation of *p*-benzyne:

$$\Delta H_f = 48.8 - \Delta H^{298}_{rxn}(\text{kcal/mol})$$

At the UB3LYP/6-31+G* level, $\Delta H^{298}_{rxn} = -86.34$ kcal/mol. This method is analogous to that used by Schleyer, Houk, Warmuth, et al. for the calculation of the heat of formation of *o*-benzyne (see ref 43).

(43) Jiao, H.; Schleyer, P. v. R.; Beno, B. R.; Houk, H. N.; Warmuth, R. *Angew. Chem., Int. Ed. Engl.* **1997**, *36*, 2761. According to these authors, the heat of formation of *o*-benzyne at the B3LYP/6-311+G** level is 113.5 kcal/mol, whereas the experimental value is $\Delta H_f = 106 \pm 3$ kcal/mol. Therefore, our estimate for the ΔH_f value of *p*-benzyne has an error smaller than that found with a benzyne of much lower biradical character.

(44) For recent DFT studies on cyclic enediynes see: (a) Schreiner, P. R. *J. Chem. Soc., Chem. Commun.* **1998**, 483. (b) Schreiner, P. R. *J. Am. Chem. Soc.* **1998**, *120*, 4184.

the reactant and only one new σ bond is formed in this reaction, we computed the R_{av} value reported in Table 1 using eq 9. Both the NICS/$NICS_{max}$ and $\sigma_{zz}^d/\sigma_{max}^d$ vs z profiles are reported in Figure 6B. From these data, it is clear that **TS3** exhibits in-plane aromatic character, the diamagnetic shielding being maximum at the molecular plane. This kind of aromaticity derives from the mixing of the σ and in-plane π frameworks.[39c] However, because the NICS decay is slightly slower than that predicted by eq 4, a small contribution from the incipient π aromaticity of *p*-benzyne being formed cannot be ruled out.

Conclusions

In-plane aromaticity seems to be a general feature of reactant-like transition structures associated with pericyclic reactions.[45] This kind of aromaticity also may be present in nonplanar transition states. We have also shown that the ring current model provides an intuitive physical image of in-plane aromaticity. In addition, this model permits the characterization of in-plane and π aromaticity. The former exhibits a maximum diamagnetic shielding at the molecular plane and decays above and below such a plane. In contrast, in π-aromatic systems the high value of the σ_{zz}^d at the ring point of electron density is not the actual maximum. The highest value of the σ_{zz}^d is reached at a certain distance above and below the molecular plane. This distance corresponds to the covalent radii of the involved atoms. This behavior is quite similar to that of the NICS values.

Finally, it is noteworthy that there does not appear to be a straightforward relationship between the magnitude of the aromaticity of the transition states of different pericyclic reactions and the activation parameters. The three reactions described in this paper range from a very easy process (reaction 2) to a probably impossible one (reaction 1). However, the corresponding transition structures are highly aromatic in character, and the features of their aromaticities seem to be very similar. The relationship between the in-plane aromatic character of a given pericyclic reaction and relevant variables such as regioselectivity, stereoselectivity, and solvent effects is unknown.

Acknowledgment. The present work has been supported by the Gobierno Vasco/Eusko Jaurlaritza (Project GV 170.215-EX97/11) and by the Secretaría de Estado de Universidades, Investigación y Desarrollo (Project PB96-1481). We also thank the CIEMAT for a generous gift of computing time on the CRAY YMP-EL computer. I.M. gratefully acknowledges the Gobierno Vasco/Eusko Jaurlaritza for a grant.

Supporting Information Available: Total energies, zero-point vibrational energies, Cartesian coordinates, and figures of all the stationary points of the reactions 1−3. This material is available free of charge via the Internet at http://pubs.acs.org.

JO981862+

(45) One reviewer has indicated that this in-plane aromatic character may be related to the reactant-like nature of the transition structures included in this work. According to his opinion, it would be interesting to scrutinize also reactions with product-like transition structures. We agree with this appreciation, and we are currently investigating this kind of reactions, in which an aromatic ring is generated. These additional studies are underway in our laboratory and will be published separately.